ISSN 1392-1207. MECHANIKA. Vol. 31, No. 3, 2025: 220–229

Multi-Objective Optimization and Design of Hydraulic and Hemolysis Performance of Micro-Axial Heart Pump

Xiaohu SANG*, Yalin SHU, Yuwen DING***, Qianli ZHAO**, Aihua XU**, Kunju SHI**, Fuhai CAI**, Dongli SHI**, Chen YANG**, Qiongyan SHI**, Chunhui LUO**, Xinping WU**, Shuo LANG**, Peishan RAO**, Feng ZHOU******

**Changzhou Vocational Institute of Mechatronic Technology, 213164 Changzhou, China, E-mail: sangxh7@qq.com (Corresponding Author)*

***Changzhou Vocational Institute of Mechatronic Technology, 213164 Changzhou, China, E-mails: 2960477106@163.com, huaren65445@sina.com, 726127910@126.com, shikunjv@sina.cn, 3031622681@qq.com, 1991@czimt.edu.cn, yangchen852@163.com, 1477603539@qq.cm, 18352861684@163.com, 947199637@qq.com, 460683181@qq.com, 3366941875@qq.com*

****Changzhou Institute of Technology, 213032 Changzhou, China, E-mail: dyw0125@qq.com*

*****Jiangsu Yaokun Hydraulic Co., Ltd., 214444 Wuxi, China, E-mail: zhoufeng123@qq.com*

https://doi.org/10.5755/j02.mech.39230

1. Introduction

Hemolysis is an important index to measure the performance of heart pump, more and more researchers explore the difference of hemolysis performance of artificial heart pump with different structure. Ardakani, K. Y., et al. [1] studied on three design parameters of artificial heart pump, clearance distance, blade height and export position relative to the blade, the larger height of the blade and the smaller gap could cause higher hemolysis index value and the gap has more obvious influence on hemolysis than the height of the blade. Li H. Y., et al. [2] designed five types of pumps with different blade thickness distributions from leading edge to trailing edge, and used Reno mean Navier-Stokes method to couple the *k-ω* sst turbulence model to influence the blade thickness, the thick blades near the leading edge restrain the flow separation between the impeller blades and improve the hydraulic efficiency at low flow rate. The blade thickness near the trailing edge changes the interaction between the volute tongue. Wiegmann L., et al. [3] studied the clearance, the number of impeller blades, and the design range of semi-open and closed shroud, the degree of stagnation and recirculation within the pump decreases, but increases as the clearance decreases. Fuwen Liu et al. [4] established a high rigid axis-solid interaction (FSI) model for roller pump in order to optimize the structure and reduce the degree of traction pulsation, and verified the accuracy of the model by experiments, on this basis, two methods of optimizing pump rotor structure are proposed. Hosseini S.E., et al. [5] in order to investigate the effects of different geometric and operational parameters of centrifugal heart pump (CBP) impellers on pump performance, including the effects of temperature, Surface roughness and the addition of inducer inducers, at the design point, the head pressure increases as the temperature increases, and the head height depends on the roughness of the impeller and decreases with the increase of the Surface roughness. The effect of CBP impeller Surface roughness is significant at high friction loss. Although the inducer installed on the pump has no significant effect on its overall performance, the wall shear stress on the impeller decreases significantly. Li W.D., et al. [6] optimized the structure of the diversion cone at the impeller inlet, effectively reducing hydraulic impact losses at the inlet and enhancing anti-hemolytic performance. Wu J.C., et al. [7] analyzed the influence of the gap between the blade tip and the pump casing on the hydrodynamic performance and blood damage in an artificial heart pump using the CFD method. heir results demonstrated that a 100 μm gap achieved the lowest hemolysis levels. Ghadimi B., et al. [8] employed metamodel-assisted genetic algorithm to simultaneously optimize the impeller and volute geometries of a typical centrifugal blood pump. The results showed that the blade inlet and outlet angle play a significant role in pump efficiency and HI. Hence, one can reduce the blade outlet angle to increase the pump efficiency and decrease the HI. Yildizeli A., et al. [9] emphasized research into the effects of design parameters for selected variations of pump blades are studied, the effects of blade's aspect ratio blade's camber angle, and the number of rotor blades were chosen as design parameters, it was shown that the most dominant parameter is the aspect ratio of the blade. The least influential parameter, camber angle, shows that the flat blade design performs better than the curved blade design examined in this study. Xiao Y.P., et al. [10] employed CFD to investigate the impact of varying clearance dimensions on the hemodynamic efficiency and hemolytic performance of a blood pump. The study demonstrated that optimizing the pump's clearance configuration significantly enhances overall pump performance. Wang C., et al. [11] utilized CFD to analyze the effects of blade fillet design in an FDA standard centrifugal blood pump on flow field characteristics and hemolytic performance, the results demonstrated that implementing fillet modifications on the impeller significantly enhances the pump's overall performance. He Y.C., et al. [12] proposed an optimized integrated axial-flow blood pump as the research subject. Using CFD, the team enhanced its geometric structure, demonstrating superior pressure head performance in the novel design. Under optimal operating conditions (rotational speed: 9000 r/min; flow rate: 6.24 L/min), the optimized pump achieved: 16% increase in pressure head compared to the original structure, 25% hydraulic efficiency, meeting physiological demands for most clinical scenarios. Liu, et al. [13] employed a Lagrangian discrete particle motion simulation method to numerically investigate the effects of pump head, rotational speed, impeller outlet angle, inlet angle, and blade number on thrombus

formation in blood pumps. The results demonstrated that the lowest thrombogenic risk was achieved with an impeller inlet angle of 30°, outlet angle of 20° and 6 blades, providing critical geometric optimization guidelines for semi-open impeller blood pumps and establishing a theoretical foundation for subsequent in vitro experiments. Jansen, et al. [14] developed an adaptive blood pump with dynamically adjustable blade parameters (including outlet/inlet angles), demonstrating superior performance versus conventional rigid pumps: 47% increase in pressure head (1.5-9.5 l/min flow range), 7.3% improvement in hydraulic efficiency.

The above mentioned optimization of heart pump is mostly to study the effect of single parameter on hemolysis performance, but less to multi-objective optimization. There are many geometric parameters of the artificial heart pump, and there is obvious interaction between them. The single-objective optimization may decrease the hydraulic performance of the artificial heart pump while optimizing the hemolysis performance, therefore, it is necessary to propose a rapid and effective multi-objective optimization method, which can simultaneously optimize the hydraulic and hemolytic performance of heart pump.

This study investigates the influence of structural parameters on hydraulic performance and hemolytic performance in an artificial heart pump using CFD. By integrating feature selection algorithms with the Response Surface method, fitting relationships between significant structural parameters and target functions (efficiency, head, and hemolysis index) are established. A multi-objective optimization of the artificial heart pump is implemented using the NSGA-II algorithm to determine the optimal combination of structural parameters.

2. Materials and Methods

2.1. Geometry

According to the normal physiological needs of the human body, for adult patients, the heart pump needs to increase the blood pressure by 100 mmHg while providing a flow rate of 5-6 l/min [15]. Suppose the impeller speed, n = 6000 r/min， As shown in Fig. 1, the current design of VAD is based on the geometry optimization of the previous pump designed in our lab [16]. The experimental *NIH* calculated for the previous model was 0.0386 g/100·l, which is quite high for a heart pump. Design improvement suggestions were made and implemented in the design reviewed in this article.

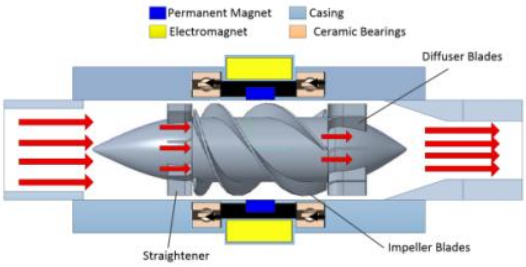

Fig. 1 Schematic diagram of the micro-axial heart pump model

2.2. Numerical simulation

The flow in the heart pump was assumed to be incompressible, turbulent, and Newtonian. The physical properties of the fluid were set to mimic human blood, with a density of 1060 kg/m^3 and viscosity of 0.0036 kg/m^2·s [17]. ANSYS Fluent was used for analysis, the damage index and shear stress was defined by the user-defined functions.

The moving reference frame, or frozen rotor technique was used for hydraulic performance analysis. The computational fluid domain was split into a rotational domain surrounding the impeller and the rest stationary domain. Interfaces were used to join these blocks. The turbulent flow option of the shear stress transport (SST) *k-ω* model was selected. The mass rate of flow at the inlet was assumed to be 5 L/min (normal cardiac efficiency level). The level of static pressure at the outlet was taken to be zero. All other boundaries are treated as no-slip wall. The inlet and outlet ports were extended to allow the incoming flow to fully develop and reduce the influence of the outlet boundary conditions. The boundary conditions and simulation methods used in this paper are shown in Table 1.

Table 1
The simulation methods and boundary conditions

Numerical solution methods	
Turbulence model	SST *k-ω*
The near-wall treatment	Enhanced
Discrete scheme of convective term	Second-order upwind scheme
Scheme of pressure-velocity coupling	SIMPLE
Inlet	Mass flow rate
Outlet	Static pressure
Turbulence model	SST *k-ω*

2.3. Hemolysis estimation model

To estimate the hemolysis, a power-law model presented by Giersipen et.al could be considered [18]. The induced mechanical blood damage (D) is directly related to scalar shear stress and exposure time and can be shown in Eq. (1)

$$D = C\tau^{\alpha} t^{\beta}, \tag{1}$$

where τ is scalar shear stress, t is exposure time, and C, α, β are experimental parameters. The constant value used is the power law constants in this paper reported in reference [9], $C = 3.62e^{-7}$, $\alpha = 2.416$, $\beta = 0.785$.

In Eq. (1), the scalar shear stress τ is

$$\tau = \sqrt{\left[\frac{1}{6}\sum\left(\tau_{ii} - \tau_{jj}\right)^2 + \sum\tau_{ij}^2\right]}, \tag{2}$$

where τ_{ij} is the stress tensor, μ is the viscosity and ρ is the density,

$$\tau_{ij} = \beta\left(\frac{\partial u_i}{\partial x_i} + \frac{\partial u_j}{\partial x_j}\right) - \rho\overline{u_i}\,\overline{u_j}. \tag{3}$$

The transport equation [19] is obtained by defining the linear hemolysis indicator $D_I = D^{1/\alpha}$ and taking the total derivative of the D_I relative to time

$$\frac{dD_I}{dt}=\left(\frac{\partial}{\partial t}+V\bullet\nabla\right)D_I=\sigma\,, \tag{4}$$

where V is the velocity vector, the source item σ is the hemolysis destruction rate in unit time

$$\sigma=\left(3.62\times10^{-7}\right)^{\frac{I}{0.785}}\tau\,. \tag{5}$$

The transient Eulerian approach in which the computation of blood damage along the pathlines is replaced by volume integration of a damage function over the computational domain was implemented [20, 21]. This method eliminates the problems associated with particle tracking, such as incomplete tracer particles. The linear damage generated by the device is calculated using the equation:

$$\overline{D_I}=\frac{1}{Q}\int_V\sigma dv\,, \tag{6}$$

where Q is the volume flow rate. The hemolysis value was obtained by exponential transform, i.e.

$$D=\overline{D_I}^{\,0.785}\,. \tag{7}$$

The numerical *NIH* level was calculated using Eq. (8) [20]:

$$NIH=Hb\times D\times100\,, \tag{8}$$

where Hb represents the hemoglobin content in the blood, Hb = 140 g/L.

3. Optimization Parameters

As shown in Fig. 2, the design of experiment (DOE) method and the optimization algorithm were used. The first step was to select the design variables according to the importance lever of the design targets and variables to the goals themselves. In the second step, the distance correlation coefficient is the evaluation criterion to measure the performance of the impeller by Optimized Space-filling Design method (OSFD). In the third step, the efficiency of each case was predicted by numerical simulation and they are selected as optimization objectives. In the fourth step, the mathematical relationships between objectives and design variables were established by using Response Surface model (RSM). In the last step, multi-objective genetic algorithm was used to solve the mathematical functions, and the optimal combination of design parameters could be obtained.

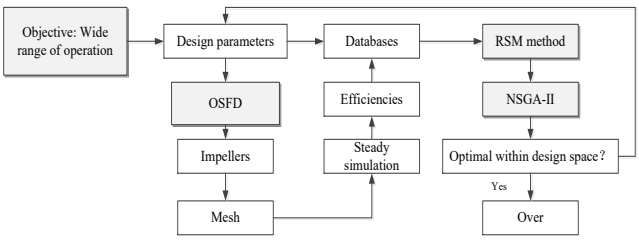

Fig. 2 Flow chat of optimization process

3.1. Design variables

The following parameters were selected as controlled (Fig. 3): impeller length L, outlet impeller diameter D_2, blade angle β_1 at the impeller inlet, blade angle β_2 at the impeller outlet, blade thickness δ, number of impeller blades Z_1 and number of impeller blades Z_2.

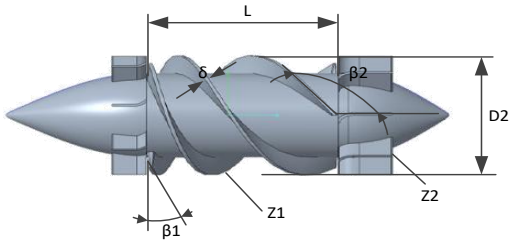

Fig. 3 Optimization parameters

3.2. Optimization objectives

The pump head and efficiency are calculated as follows:

$$H=\frac{p_2-p_1}{\rho g}+\frac{v_2^2-v_1^2}{2g}\,, \tag{9}$$

$$\eta=\frac{\rho gQH}{P}\,. \tag{10}$$

Besides, NIH level was calculated using Eq. (8), where, p_2 and p_1 are the static pressures measured at the outlet and inlet; v_2 and v_1 are the velocities at the outlet and inlet; g is the gravity; P is the input power of the pump.

4. Results and Discussions

4.1. Mesh generation

The meshing tool ANSYS meshing generates a grid, and the hexahedral structured grid is used for the inlet section and outlet section. Due to the complex geometry of impeller and diffuser blades, unstructured tetrahedral grids with strong adaptability are selected in these domains. Because the blood flow in the impeller and diffuser belongs to turbulent flow, to ensure the calculation accuracy, the hexahedral grid boundary layer is divided on the wall of the impeller and diffuser to ensure that the y^+ value of the first grid of the wall boundary layer is less than 1.

Table 2 shows the predicted pressure head, hydraulic efficiency, and hemolysis index for grid sensitivity analysis of the simulation studies. Four sets of grids with different grid numbers are given, it can be seen from the table that the difference in heart pump head calculated by grid 3 and grid 4 is 0.21 mmHg, the hydraulic efficiency is different by 0.11%, the maximum difference in hemolysis index is 0.0002, and the relative errors are all less than 0.5%. To save computing resources and improve computing speed while maintaining accuracy, this paper uses grid 3 as the grid scale for subsequent research to carry out numerical simulation calculations.

To verify the numerical simulation method in Table 1, FDA centrifugal heart pump is used for verification in this paper. CFD simulation calculation is carried out for the

Table 2

Grid sensitivity analysis

Conditions	Grid No.	Grid, Mn	y^+_{max}	P, mmHg	η, %	NIH, g·(100 L)$^{-1}$
5 L/min, 6000 rpm	1	2.57	0.85	107.3	72.7	0.0306
	2	3.89	0.59	106.7	71.1	0.0343
	3	4.27	0.26	106.4	71.2	0..0346
	4	5.63	0.24	106.6	71.3	0.0348

Table 3

FDA's benchmark heart pump operating conditions

Conditions	Mass flow rate, L/min	Pump speed, rpm
1	2.58	2500
2	2.58	3500
3	4.68	3500
4	6	2500
5	6	3500

six working conditions in Table 3 and compared with the experimental results provided in Ref. [22].

The comparison results of flow-head distribution are shown in Fig. 4. It can be seen that the numerical simulation results in this paper are relatively consistent with the experimental data. The maximum relative error with the experimental data is less than 6%, indicating that the simulation method used in this paper is acceptable.

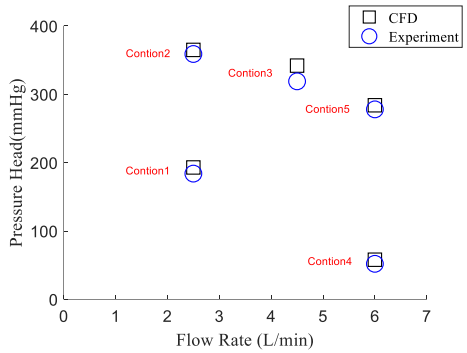

Fig. 4 FDA heart pump performance comparison

4.2. Multi-objective optimization

4.2.1. Effect of the main structural parameters of the impeller on the performance

Fig. 5 shows the efficiency increases with the impeller outlet diameter D_2, and the efficiency is highest when the impeller outlet diameter D_2 reaches 17 mm, and then decreases with the impeller outlet diameter, head and *NIH* both increase with the impeller outlet diameter. Excessive value of the impeller outlet diameter will increase the absolute speed of the impeller outlet, impeller detachment, and cardiac force and shear stress will increase, lead to increased impact loss at the guide vane inlet, reduce the efficiency of the heart pump, and improve the head and *NIH*.

Fig. 6 shows the efficiency increases with the impeller length, and the efficiency is highest when the impeller length reaches 20 mm, and then decreases with the impeller length, head and *NIH* both decrease with the impeller length. Excessive value of the impeller outlet diameter will increase the absolute speed of the impeller outlet, impeller detachment, and cardiac force and shear stress will increase, lead to increased impact loss at the impeller inlet, reduce

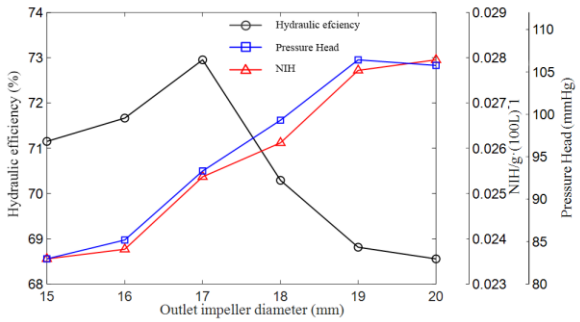

Fig. 5 Effect of the impeller outlet diameter on the performance of the heart pump

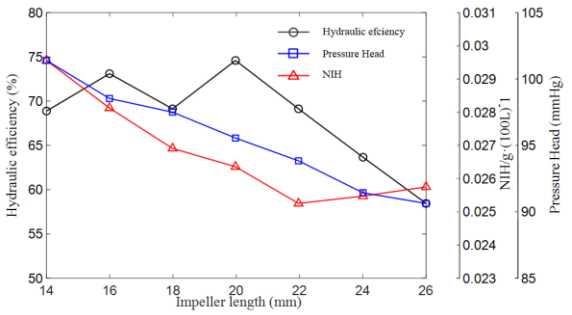

Fig. 6 Effect of the impeller length on the performance of the heart pump

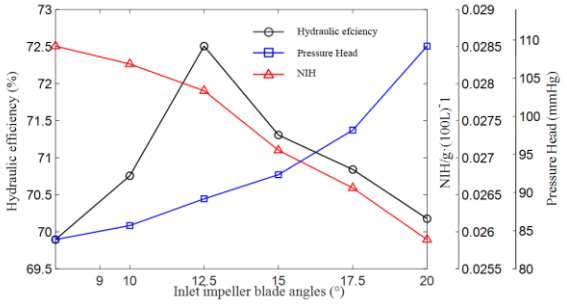

Fig. 7 Effect of the inlet impeller blade angles on the performance of the heart pump

the efficiency of the heart pump, and improve the head and *NIH*.

Fig. 7 shows the efficiency increases with increasing inlet impeller angle when the inlet impeller angle is between 9° and 12.5°, the highest value is observed at the angle of 12.5°. The *NIH* decreases with the angle, and the head decreases with the increase of the angle. This indicates that after the inlet impeller angle exceeds 12.5°, the increase of the angle will aggravate the impact at the impeller entrance, increase the overflow area of the blade inlet, increase the hydraulic friction loss, and then reduce the efficiency, head and increase the *NIH*.

As shown in Fig. 8, when the impeller outlet angle

is between 20° and 30°, the efficiency increases with the increase of the outlet angle. When the blade outlet angle exceeds 30°, the efficiency decreases with the increase of the outlet angle. When the blade outlet angle is between 20° and 45°, both the head and NIH increase with the increase of the outlet angle. The increase of the blade outlet angle can reduce the friction loss between the impeller and blood, but it will increase the impact loss at the inlet of the guide vane. According to the efficiency change trend, when the outlet angle changes between 20° and 45°, the reduced friction loss is dominant, so the efficiency increases with the increase of the outlet angle in this range. When the outlet angle changes between 30° and 45°, the increased impact loss is greater than the reduced friction loss, so the efficiency decreases with the increase of the outlet angle. Increasing the blade outlet angle will increase the absolute velocity at the impeller outlet, intensify the collision between the high-speed flow at the impeller outlet and the low-speed flow in the guide vane, cause flow turbulence, and lead to an increase in the NIH value.

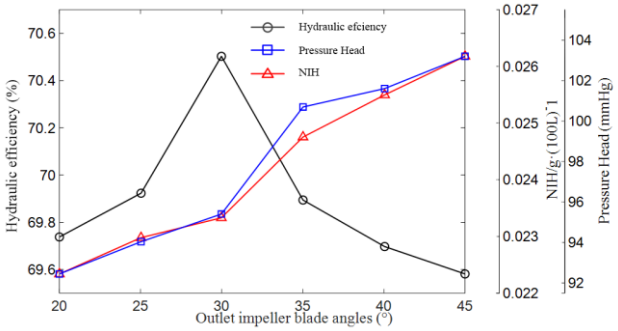

Fig. 8 Effect of the outlet impeller blade angles on the performance of the heart pump

Fig. 9 shows the efficiency increases with increasing blade thickness when the thickness is between 0.5 mm and 1.5 mm, when the blade thickness exceeds 1.25 mm, the efficiency began to decrease. When the blade thickness is between 0.5 mm and 1.25 mm, the efficiency increases with the blade thickness. When the thickness exceeds 1.25 mm, the efficiency begins to decrease. With the blade thickness between 1 mm and 1.5 mm, the pressure head decreases with the increase of the blade envelope angle. When the thickness was between 0.5 mm and 1.5 mm, *NIH* decreased with increasing thickness. This shows that the blade thickness is too large, although it will enhance the constraint of the impeller on the blood, reducing the flow separation and vortex phenomenon, it reduces the blood damage, but the growth of the flow channel increases the hydraulic friction loss, reducing the efficiency and pressure head.

Fig. 10 shows when the number of impellers is increased, the pressure head of the heart pump is increased, this is due to more blades providing greater fluid velocity and energy conversion. However, when the number of blades is too much, the impeller channel is narrowed, which may increase the flow resistance of the fluid, resulting in the decrease of the efficiency of the heart pump, because there is an optimal value of the number of blades, which can meet the requirements of the maximum efficiency of the pump. In addition, with the increase of the number of blades, the flow area of the passage increases, and the shear force

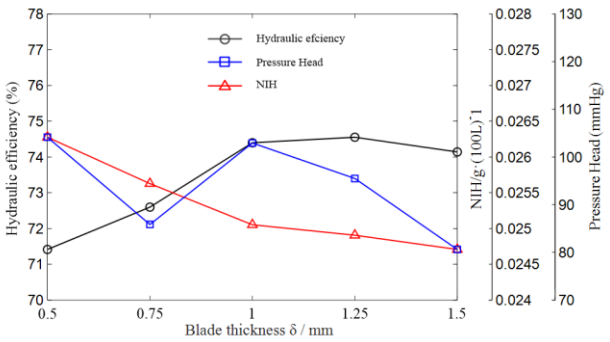

Fig. 9 Effect of the outlet blade thickness on the performance of the heart pump

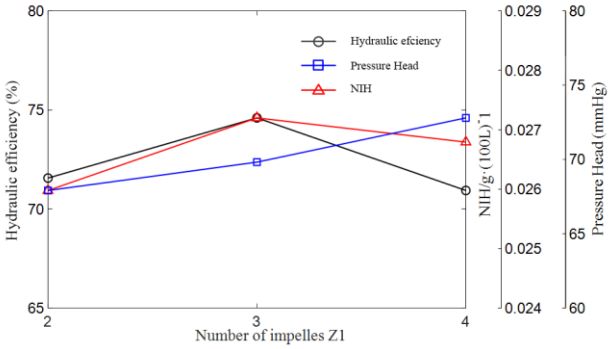

Fig. 10 Effect of the number of impeller blades on the performance of the heart pump

of the blood increases when the impeller rotates at high speed, which is easy to cause high NIH.

4.2.2. Optimize project

The response surface is an approximate estimation model of the input and output parameters based on the data group, the specific process is as follows: Firstly, a parametric three-dimensional model of the spiral maze pump is established in CREO software. Secondly, the structural parameters of the model pump are identified and controlled through the parametric function of ANSYS Workbench, and the target function requiring output is set in the fluid calculation module to establish the corresponding relationship between the structural parameters and the target function. Thirdly, the required test sites were determined using OSFD. The test sites are calculated one by one with RSM. According to the test data obtained, the mathematical model between structural parameters efficiency, hemolysis index and head is fit in the response surface and optimization module, that is, the optimization model based on the response surface. On this basis, this model is calculated by using the multi-objective genetic optimization algorithm to obtain a series of solutions that meet the requirements, and one of the solutions is selected as the final structural optimization size according to the actual engineering needs.

4.2.3. Determine the optimization parameters

Because the hydraulic performance and hemolysis index of heart pump involves 6 structural design parameters, and there are interactions between the various parameters. Table 4 shows the simplified structure design parameters and their value range.

Table 4

Range of design parameters

Dimensions	Initial value	Range
Impeller length L, mm	20	15-26
Outlet impeller diameter D_2, mm	18	15-20
Inlet impeller blade angles β_1, °	10	9-20
Outlet impeller blade angles β_2, °	30	20-45
Blade thickness δ, mm	0.5	0.5-1.5
Number of impeller blades Z_1	2	2-4

To remove the parameters that had less influence on the external characteristics of heart pump, a sensitivity analysis of the parameters was performed to select the design parameters to be optimized. In this paper, the Parameters Correlation module of ANSYS Workbench was used to obtain the sensitivity distribution of each design parameter to the optimized target. The module uses the Spearman Correlation Coefficient method to perform the parameter sensitivity analysis. This method can be used to measure the strength of the associations between the variables. The larger the absolute value means that the greater the input parameters influence the output parameters, and the positive value indicates that the output parameters are positively correlated with the input parameters. The correlation coefficient of this method is defined as shown in Eq. (11) [12, 13]

$$P_s = \frac{\sum_{i=1}^{N}\left(R_i-\tilde{R}\right)-\left(S_i-\tilde{S}\right)}{\sum_{i=1}^{N}\left(R_i-\tilde{R}\right)^2\sum_{i=1}^{N}\left(S_i-\tilde{S}\right)^2} = 1-\frac{6\sum d_i^2}{N\left(N^2-1\right)}, \quad (11)$$

where R_i and S_i are the value rank of the observed values i, respectively, $\tilde{R}$ and $\tilde{S}$ are the average grades of variables x and y, respectively, N is the total number of observed values, and $d_i = R_i - S_i$ is the rank difference of pairs of variables in two columns.

Fig. 11 shows the results of the sensitivity analysis of each design parameter on the head, efficiency and hemolysis index of the heart pump. As can be seen from Fig. 10, The outlet impeller diameter is the most sensitive to the head, efficiency and hemolysis index of the pump, while the impeller length is very low sensitive to the efficiency, only –0.012, so the effect of the impeller length on the pump efficiency can be ignored. The number of impeller blade has the lower sensitivity on efficiency and head of the pump, only –0.022 and 0.019. Considering that this study focuses on improving the efficiency of the model pump, the impeller length and the number of blade are determined in the subsequent optimization process. Based on the above results, the four parameters of outlet blade angles β_2, inlet impeller blade angles β_1, outlet impeller diameter D_2 and blade thickness δ were selected as the main parameter variables for optimization.

4.2.4. Sample library construction and fitting optimization

In this paper, the RSM is selected to build the proxy model fitting optimization model, according to which

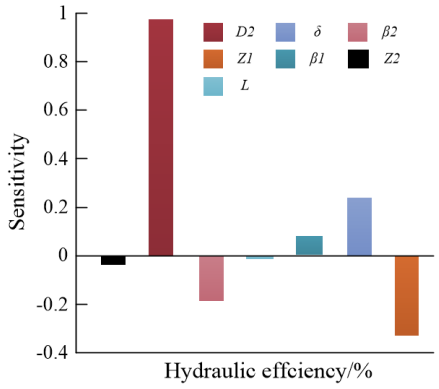

a

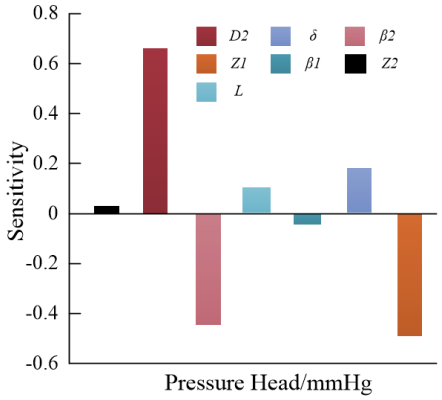

b

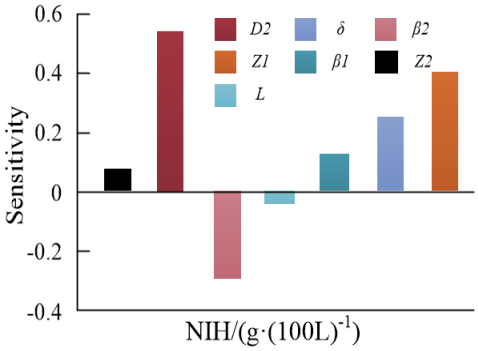

c

Fig. 11 Analysis on sensitivity of design parameters: a – efficiency, b – head, c – hemolysis index of the heart pump

the required heart pump sample points can be calculated by numerical simulation. The sample library construction of the fitted model was performed using Box-Behnken design, and Box-Behnken design enabling efficient estimation of first and second order coefficients in the RSM. Table 5 shows the three-level of the structural parameters.

The performance results of the numerical calculation of the 30 sample points and the heart pump in Table 6 are obtained by Design Expert software.

4.2.5. Response surface test

The data in Table 7 are processed using Design-Expert software and the variance analysis results for sample points are shown in Table 5. It can be seen that the fitted

model Signal-to-noise ratio of the head is greater than 4.0, the model *Prob* > *F* is less than 0.0001, the regression determination coefficient R^2 = 0.9971 and the corrected regression determination coefficient R_{adj}^2 = 0.9932, the fit of the sample point model can be considered reliable. The signal to noise ratio of the hydraulic efficiency model is also greater than 4.0, the model *Prob* > *F* is less than 0.0001, and the difference between the regression determination coefficient R^2 and the corrected regression determination coefficient R_{adj}^2 is less than 0.2. The fitted hydraulic efficiency model can also be used for optimization design.

4.3. Multi-objective optimization model and solution

Fig. 12 shows the influence of the four structural parameters of *A, B, C*, and *D* on the performance of the heart pump. According to the curve, the parameter *C*, the outlet impeller blade angles, is more obvious on the hydraulic efficiency of the heart pump than the other three parameters. However, the parameter outlet impeller diameter *A*, inlet impeller blade angles *B*, and blade thickness *D* all have obvious effects on the head of the pump. The regression equation between the head stage of the pump *H*, hydraulic efficiency η, hemolysis index *NIH* and the structural parameters D_2 (*A*),

Table 5

Test the level and coding of each structural parameter

Factors	Three-level		
	-1	0	1
A: Outlet impeller diameter D_2, mm	15	18	20
B: Inlet impeller blade angles β_1, °	10	15	20
C: Outlet impeller blade angles β_2, °	20	30	45
D Blade thickness δ, mm	0.25	0.5	1

Table 6

Sample point design and numerical results

No	A	B	C	D	Hydraulic Efficiency	Pressure Head, mmHg	*NIH*, g·(100L)$^{-1}$
1	-1	-1	0	0	0.70	66.02	0.022
2	1	-1	0	0	0.72	75.25	0.0225
3	-1	1	0	0	0.71	102.35	0.0265
4	1	1	0	0	0.71	103.21	0.0235
5	0	0	-1	-1	0.69	100.23	0.0231
6	0	0	1	-1	0.75	90.25	0.0271
7	0	0	-1	1	0.71	86.42	0.0263
8	0	0	1	1	0.72	88	0.0242
9	0	-1	0	0	0.73	87.21	0.0255
10	0	1	0	0	0.69	86.3	0.0233
11	0	-1	0	0	0.72	90.5	0.0236
12	0	1	0	0	0.71	91.25	0.0275
13	-1	0	-1	0	0.69	84.21	0.0261
14	1	0	-1	0	0.69	94.16	0.0228
15	-1	0	1	0	0.72	92.35	0.0236
16	1	0	1	0	0.71	99.9	0.0254
17	0	0	0	-1	0.74	100	0.0263
18	0	0	0	1	0.72	102.3	0.0272
19	0	0	0	-1	0.69	101.7	0.0266
20	0	0	0	1	0.73	94.2	0.0257
21	0	-1	-1	0	0.71	98.6	0.0234
22	0	1	-1	0	0.72	86.52	0.0275
23	0	-1	1	0	0.74	88.32	0.0288
24	0	1	1	0	0.73	104.3	0.0265
25	-1	0	0	-1	0.69	97.7	0.0277
26	1	0	0	-1	0.68	100.2	0.0232
27	-1	0	0	1	0.72	72.56	0.0238
28	1	0	0	1	0.73	105.32	0.031
29	0	0	-1	0	0.71	95.65	0.0285
30	0	0	1	0	0.72	99.2	0.0246

Table 7

Variance analysis of Model sample point

Project	Mean square			R^2	R_{adj}^2	Signal noise ratio
	fitted model	Fitting deviation	error term			
Pressure Head	9379.02	0.0516	4.6e^{-6}	0.9971	0.9932	90.7384
Hydraulic Efficiency	6.018e^{-3}	0.0079	2.2e^{-6}	0.9583	0.8813	94.1096
NIH	4.237e^{-4}	0.0063	4.8e^{-6}	0.9932	0.9846	92.0231

β_1 (*B*), β_2 (*C*), δ (*D*) is established as follows:

$$\begin{aligned}\eta = F_1 = {} & 0.436 + 0.153A + 1.898e^{-3}B + \\ & +0.0123C - 1.721e^{-4}D - 6.425e^{-3}AB - \\ & -4.839e^{-4}AC - 1.599e^{-4}AD - 0.025BC + \\ & +1.112e^{-3}BD - 0.372e^{-4}CD - 0.362e^{-3}A^2 - \\ & -2.482e^{-5}B^2 + 0.476C^2 - 1.599D^2 \end{aligned} , \quad (12)$$

$$\begin{aligned}H = F_2 = {} & 350.735 - 7.352A - 3.056B - \\ & -123.56C - 32.35D + 0.039AB + \\ & +0.712AC + 0.351AD - 0.176BC + \\ & +1.12BD - 0.357CD + 0.126A^2 + \\ & +6.721e^{-3}B^2 + 22.653C^2 - 12.63D^2 \end{aligned} , \quad (13)$$

$$\begin{aligned}NIH = F_3 = {} & 0.0894 - 3.583e^{-4}A - \\ & -3.683e^{-4}B - 0.0593C - 0.0238D - \\ & -1.264e^{-5}AB + 7.586e^{-5}AC + \\ & +0.125e^{-5}AD - 2.893e^{-5}BC + \\ & +2.397e^{-5}BD - 5.238e^{-5}CD + 1.556e^{-5}A^2 + \\ & +5.126e^{-6}B^2 + 7.012e^{-3}C^2 + 3.235e^{-4}D^2 . \end{aligned} \quad (14)$$

The optimization test objective constraints and optimization objectives are as follows Eq. (15). According to the relationship between the centrifugal pump performance and structural parameters Eqs. (12)-(14), the set of structural parameters that meet the head of 96.3 mmHg and the maximum hydraulic efficiency, the minimum hemolysis index *NIH* are found by Design-Expert software within the constraint range of the structural variables. The optimized structure parameters are obtained as follows: The outlet impeller

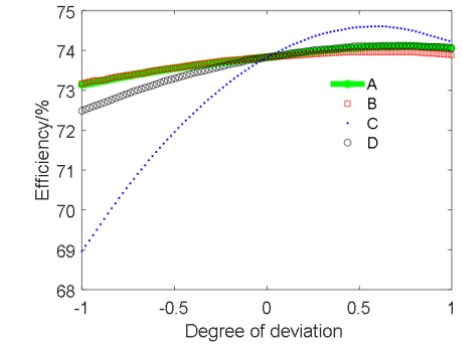

a

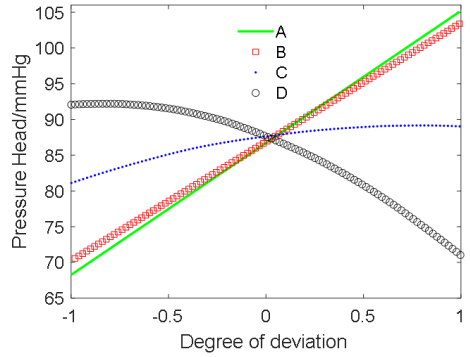

b

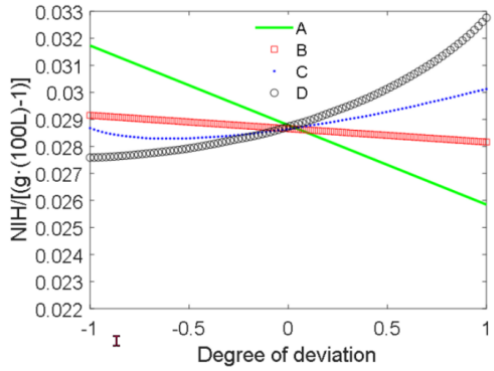

c

Fig. 12 Effect of the test parameters on the performance parameters of the heart pump: a – efficiency, b – pressure head, c – hemolysis index

blade angles is $\beta_2 = 30°$, the outlet impeller diameter is $D_2 = 20$ mm, the outlet impeller blade angles is $\beta_1 = 12.5°$, and the blade thickness is $\delta = 1$ mm.

The optimization mathematical model was established with maximizing efficiency and head and minimizing *NIH* value as the optimization objectives:

$$\begin{cases} min\, F = [-F_1, -F_2, F_3] \\ s.t.[A, B, C.D] \\ A \in [15, 20] \\ B \in [10, 20] \\ C \in [20, 45] \\ D \in [0, 25, 1] \end{cases} . \quad (15)$$

According to Fig. 13, the theoretical calculated values of the original model and the optimized model are quite close to the CFD simulation values, which demonstrates the effectiveness of the adopted response surface method optimization method combined with the NSGA algorithm. Compared with the original model, the head of the optimized model is 96.3 mmHg, which increased compared with the original model, and just met the normal physiological needs of human body, the hydraulic efficiency increased by 3%, and the hemolytic value *NIH* decreased by 27%, the optimization degree was high. Compared with the new heart pump developed in literature [23], the *NIH* value of the optimized model was 0.0172 g/100·L in the same working conditions, which is much lower than the hemolysis value of the new heart pump in literature [23], proving the effectiveness of the optimized method in this paper.

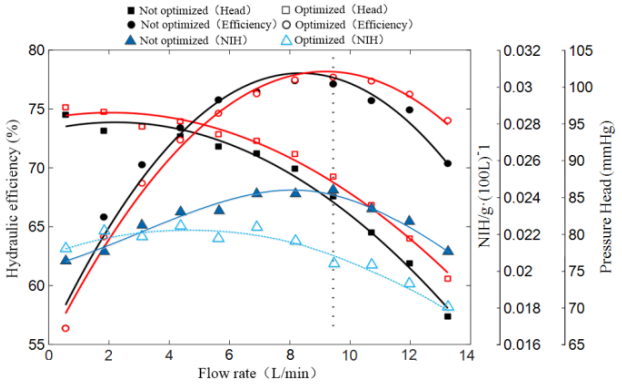

Fig. 13 Performance comparison between the optimized model and the original model

5. Conclusions

1. The influence of the structural parameters of heart pump on their performance was analyzed by CFD, and four significant parameters were selected as design variables by single target feature selection method, namely outlet impeller diameter D_2, inlet impeller blade angles β_1, outlet impeller blade angles β_2 and blade thickness δ.

2. By the Box-Behnken test design method and the CFD numerical simulation, the test sample point and the corresponding performance parameters were obtained. Using Design-Expert software, the results of variance analysis showed that the regression models fit well, It can be used to guide the design space.

3. To solve the regression equation by the NSGA-multi-objective algorithm, Best outlet structure parameters of selected heart pump: $\beta_2 = 30°$, $D_2 = 20$ mm, $\beta_1 = 12.5°$, $\delta = 1$ mm. Performance parameters of the heart pump under working condition: efficiency is 74.5%, the head is 96.3 mmHg, the hemolytic value is 0.0172 g·(100L)$^{-1}$, the hydraulic efficiency and hemolysis values are better to the original model.

Author Contributions: The contributions of all the authors to this manuscript are as follows: X.H.S., Y.L.S., Y.W.D., Q.L.Z., A.H.X., K.J.S., F.H.C., D.L.S. and C.H.L. designed the study and wrote the protocol; F.Z. provided the equipment (sensors, high-performance workstation, et al) and extracted the data; S.L. and X.P.W. conducted the statistical analysis; X.H.S., A.H.X., K.J.S., Y.L.S. and D.L.S. wrote the first draft of the manuscript. All authors commented on

previous versions of the manuscript. All authors have read and agreed to the published version of the manuscript.

Funding: This research was supported by Changzhou Sci&Tech Program, Grant No. CJ20230014, CJ20240019; Jiangsu Industry Academia Research Cooperation Project, Grant No. BY20231152; The High-end training program for leading teachers in vocational colleges in Jiangsu Province, Grant No. 2023GRFX006; QingLan Project of Jiangsu Province.

Data Availability Statement: The raw data supporting the conclusions of this article will be made available by the authors on request.

Acknowledgments: Acknowledgements to Jiangsu Yaokun Hydraulic Co., Ltd., for support of the test site and equipment for this research subject.

Conflicts of Interest: The authors declare no conflicts of interest.

References

1. **Yazdanpanah-Ardakani, K.; Niroomand-Oscuii, H.; Kanan, R. S. K.; Shokri, N.** 2024. Optimization of a centrifugal heart pump designed using an industrial method through experimental and numerical study, Scientific Reports 14: 7443. https://doi.org/10.1038/s41598-024-57019-9.
2. **Li, H. Y.; Zhang, M. K.; Luo, X. W.; Wu Q. Y.** 2023. Investigation on the effects of blade thickness for a centrifugal rotary heart pump, Journal of Mechanical Science and Technology 37(2), 767-778. https://doi.org/10.1007/s12206-023-0120-7.
3. **Wiegmann, L.; Boës, S.; de Zélicourt, D.; Thamsen, B.; Schmid Daners, M.; Meboldt, M.; Kurtcuoglu, V.** 2018. Blood pump Design Variations and Their Influence on Hydraulic Performance and Indicators of Hemocompatibility, Annals of Biomedical Engineering 46: 417-428. https://doi.org/10.1007/s10439-017-1951-0.
4. **Liu, F.; Li, Q.; Gong, Z.; Zhang, Y.; Song, X.** 2024. Structure optimization design of extracorporeal circulation blood transport pump, Structural and Multidisciplinary Optimization 67: 37. https://doi.org/10.1007/s00158-024-03762-6.
5. **Hosseini, S. E.; Keshmiri, A.** 2022. Experimental and numerical investigation of different geometrical parameters in a centrifugal blood pump, Research on Biomedical Engineering 38: 423-437. https://doi.org/10.1007/s42600-021-00195-8.
6. **Li, W.; Yao, Q; Du, J.; Zhou, C.; Niu, Y.** 2017. Optimizationan alysis for impeller inlet of artificial heart pump with hydraulic suspension based on CFD, Beijing Biomedical Engineering 36(1): 21-28.
7. **Wu, J. C.; Paden, B. E.; Borovetz H. S., Antaki, J. F.** 2010. Computational Fluid Dynamics Analysis of Blade Tip Clearances on Hemodynamic Performance and Blood Damage in a Centrifugal Ventricular Assist Device, Artificial Organ 34(5): 402-411. https://doi.org/10.1111/j.1525-1594.2009.00875.x.
8. **Ghadimi, B.; Nejat, A.; Nourbakhsh, S. A.; Naderi, N.** 2019. Shape optimization of a centrifugal blood pump by coupling CFD with metamodel-assisted genetic algorithm, Journal of Artificial Organs 22: 29-36. https://doi.org/10.1007/s10047-018-1072-z.
9. **Yildizeli, A.; Alver, M. T.; Celik, A.; Yurduseven, M.; Cadirci, S.** 2025. Effect of the design modifications on the hemocompatibility and hydrodynamic performance of FDA-approved blood pump at various operating conditions, Research on Biomedical Engineering 41: 20. https://doi.org/10.1007/s42600-025-00403-9.
10. **Xiao, Y. P.; Xiao, Y.; Cao, Z. S., Lian, Q. L.; Cui, G. M.; Wang, J. Y.** 2025. Analysis on Efficiency and Hemolysis Performance of Centrifugal Blood Pump with Axial Clearance, Journal of Medical Biomechanics 40(2): 404-411. https://doi.org/10.16156/j.1004-7220.2025.02.021.
11. **Wang, C.; Polin, H.; Wu, P.** 2019. Effects of Rounding on Prediction of Flow Field and Hemolysis for the FDA Benchmark Blood Pump, Journal of Medical Biomechanics 34(1): 58-63. https://doi.org/10.16156/j.1004-7220.2019.01.009.
12. **He, Y. C.; Qiu Y. X.; Zhang Y., Cui, Y. X.; Dianyu, E.** 2024. Simulation and optimization of integrated axial flow blood pump system, Chinese Journal of Medical Physics 41(9): 1152-1162. https://doi.org/10.3969/j.issn.1005-202X.2024.09.014.
13. **Liu, X.; Shao, J.; Wang, P.; Zhao, H.; Liu, L.; Han, Q.** 2024. Optimization design of semi-open impeller based on thrombogenicity in a blood pump. Artif Organs 48(9): 1060-1069. https://doi.org/10.1111/aor.14813.
14. **Jansen, S. V.; Heinemann, C.; Schüller, M.; Schmitz-Rode, T.; Steinseifer, U.** 2024. Toward an Adjustable Blood Pump for Wide-Range Operation: In-Vitro Results of Performance Curve and Hydraulic Efficiency, ASAIO Journal 70(7): 579-585. https://doi.org/10.1097/mat.0000000000002163.
15. **Baldwin, J. T.; Adachi, I.; Teal, J.; Almond, C. A.; Jaquiss, R. D.; Massicotte, M. P.; Dasse, K.; Siami, F. S.; Zak, V.; Kaltman, J. R.; Mahle, W. T.; Jarvik, R.** 2017. Closing in on the PumpKIN Trial of the Jarvik 2015 Ventricular Assist Device, Seminars in Thoracic and Cardiovascular Surgery: Pediatric Cardiac Surgery Annual 20: 9-15. https://doi.org/10.1053/j.pcsu.2016.09.003.
16. **Sang, X. H.; Zhou, X. J.; Liu, X. G.; Hao, X. R.** 2017. Radial force within two-stage axial-flow blood pump based on LES, Journal of Vibroengineering 19(2): 1332-1344. https://doi.org/10.21595/jve.2016.17537.
17. **Hara, S.; Maeno, E.; Li, X.; Yurimoto, T.; Isoyama, T. Saito, I.; Ono, T.; Abe, Y.** 2017. Principle and basic property of the sequential flow pump, Journal of Artificial Organs 20: 215-220. https://doi.org/10.1007/s10047-017-0959-4.
18. **Giersiepen, M.; Wurzinger, L.J.; Opitz, R.; Reul, H.** 1990. Estimation of Shear Stress-related Blood Damage in Heart Valve Prostheses - in Vitro Comparison of 25 Aortic Valves, The International Journal of Artificial Organs 13(5): 300-306. https://doi.org/10.1177/039139889001300507.
19. **Garon, A.; Farinas, M. I.** 2004. Fast three-dimensional numerical hemolysis approximation, Artificial Organs 28(11): 1016-1025. https://doi.org/10.1111/j.1525-1594.2004.00026.x.
20. **Pauli, L.; Nam, J.; Pasquali, M.; Behr, M.** 2013. Transient stress-based and strain-based hemolysis estimation in a simplified blood pump, International Journal for Numerical Methods in Biomedical Engineering 29(10): 1148-1160.

https://doi.org/10.1002/cnm.2576.
21. **Bludszuweit, C.** 1995. Model for a General Mechanical Blood Damage Prediction, Artificial Organs 19(7): 583-589. https://doi.org/10.1111/j.1525-1594.1995.tb02385.x.
22. **Malinauskas, R. A.; Hariharan, P.; Day, S. W.; Herbertson, L. H.; Buesen, M.; Steinseifer, U.; Aycock, K. I.; Good, B. C.; Deutsch, S.; Manning, K. B.; Craven, B. A.** 2017. FDA Benchmark Medical Device Flow Models for CFD Validation, ASAIO Journal 63(2): 150-160. https://doi.org/10.1097/MAT.0000000000000499.
23. **Wu, Y.; Zhu, L. F.; Luo, Y.** 2018. Computational Fluid Dynamics Analysis of an Injection Suspension Blood Pump on the Hydraulic, Suspension and Hemolysis Property, Journal of Mechanical Engineering 54(20): 52-58. https://doi.org/10.3901/JME.2018.20.052.

X. Sang, Y. Shu, Y. Ding, Q. Zhao, A. Xu, K. Shi, F. Cai, D. Shi, C. Yang, Q. Shi, C. Luo, X. Wu, S. Lang, P. Rao, F. Zhou

MULTI-OBJECTIVE OPTIMIZATION AND DESIGN OF HYDRAULIC AND HEMOLYSIS PERFORMANCE OF MICRO-AXIAL HEART PUMP

S u m m a r y

In order to optimize the hydraulic performance of the heart pump and reduce blood damage, the effects of the main structural parameters on efficiency, head and hemolysis values was studied by CFD, outlet impeller diameter, inlet impeller blade angles, outlet impeller blade angles and blade thickness were selected as design variables using OFSD method, the efficiency, head, and hemolytic performance of the pump were taken as objective functions, the response surface method is used to fit the multivariate regression model of design variables and objective functions. Finally, the multi-objective optimization is carried out with NSGA-II genetic algorithm, one of the qualified structural parameter combinations was selected according to actual needs as the final solution of the optimization. The outlet impeller blade angles is $\beta_2 = 30°$, the outlet impeller diameter is $D_2 = 20$ mm, the outlet impeller blade angles is $\beta_1 = 12.5°$, and the blade thickness is $\delta = 1$ mm. Efficiency is 74.5%, head is 96.3 mmHg, the hemolytic value is 0.0172 $g \cdot (100L)^{-1}$. The study results can provide a reference for the structural optimization of heart pumps.

Keywords: heart pump, structural optimization, RSM, OSFD, multi-objective optimization, NSGA.

Received October 24, 2024
Accepted June 25, 2025